Comparison of Deionized Water and FC-72 in Pool and Jet Impingement Boiling Thermal Management

Ruander Cardenas[1] and Vinod Narayanan[2]

School of Mechanical, Industrial, and Manufacturing Engineering; Oregon State University, Corvallis, OR 97331-6001

[1] email: ruander@lifetime.oregonstate.edu

[2] corresponding author, email: vinod.narayanan@oregonstate.edu; Ph: (541) 737 7012

Abstract

High heat fluxes and stringent constraints on surface temperature and its uniformity during thermal management of electrical and electronic components often necessitate use of boiling heat transfer. This study compares the pool and jet impingement boiling heat transfer characteristics of deionized water and FC-72 at an equivalent fluid saturation temperature of 57 ^{o}C and for identical experimental conditions. To lower the saturation temperature of water down to 57 ^{o}C, experiments with water are performed at a reduced absolute system pressure of 0.176 bar. Despite the reduction in pressure, pool boiling critical heat flux with deionized water is found to be 3.6 times larger than with FC-72. Furthermore, jet impingement is seen to enhance boiling heat transport more significantly for water than for FC-72. Consequently, heat transfer coefficients during jet impingement boiling are as much as 3.9 times larger for water compared to FC-72 at identical Reynolds numbers and surface temperatures. The heat transfer advantage of using water is mainly associated with the superior thermophysical properties of this fluid. However, in addition to the large fluid saturation temperature at atmospheric conditions, direct cooling of electronics is frequently not possible using water due to the incompatibility of the fluid with electrical components. To assess the practical utility of subatmospheric deionized water through indirect cooling of electronics, a one-dimensional heat sink analysis is performed on a multi-chip module geometry. The overall thermal resistance of the heat sink using water is determined to be around two times lower than that of direct cooling of FC-72 on a silicon substrate. Under saturation condition of the working fluids, dissipation of heat fluxes in excess of ~ 45 W/cm^2 with the multi-chip module with water are constrained by the chip surface temperature limit.

Index Terms (Keywords)

Boiling heat transfer, dielectric, deionized water,FC-72, jet impingement boiling, pool boiling, thermal management, heat sink, thermal resistance, electronics cooling

Introduction

Thermal management of high power electronics requires dissipation of heat fluxes in excess of 100 W/cm^2 while maintaining surface temperatures below 85 ^oC [1]. According to the International Technology Roadmap for Semiconductors (ITRS) [2], a typical maximum junction temperature for a microprocessor is about 100 ^oC and 85 ^oC for a memory device. Since devices with possibly different temperature limits are often integrated inside the same package, a maximum temperature limit of 85 ^oC is often targeted for electronics cooling applications [3-5]. Boiling heat transfer has found increasing use to satisfy this demand owing to the high heat transfer rates and relatively tight control over surface temperatures. Typically, dielectric fluids like FC-72 are used to cool such electronic devices, especially in direct contact cooling applications. As a consequence of the poor thermal transport properties of such fluids, it is often necessary to employ forced convective heat transfer schemes to augment pool boiling heat transfer rates for high flux chip cooling. These schemes take the form of microchannel convective boiling and jet impingement and spray impingement boiling.

Deionized water has superior thermal properties, including an enthalpy of vaporization that is two orders of magnitude larger than most dielectric and heat transfer fluids (see Table 1), and hence, it has the potential for use in high flux cooling applications. While the saturation temperature of water at atmospheric pressure is larger than the maximum temperature limit permissible in electronics cooling, the temperature constraint can be met by lowering the working system pressure. The chief barrier to using water for electronics cooling stems from the difficulty in keeping this fluid dielectric, thereby precluding direct contact with chip electrical interconnects in current packaging technology. One possibility that permits use of water is an indirect cooling approach wherein the cooling fluid is contained within a heat sink located on top of a chip using a thermal interface material (TIM).

With the goal of using water for electronics cooling applications, Pal and Joshi [5] studied the pool boiling heat transfer characteristics of water at subatmospheric conditions in a thermosyphon loop. The authors noted that the benefit of lower wall temperatures at subatmospheric conditions was accompanied by deterioration in wall heat flux. Nevertheless, heat fluxes in excess of 100 W/cm^2 were reported for surface temperatures below 85 ^oC. In comparison to a plain surface, structures surfaces showed improved heat transfer rates. The heat transfer rate was observed to be dependent on the liquid fill level. The authors noted that the physics of bubble formation and its dependence on pressure it's an important contributor to the observed heat transfer characteristics.

Since the normal boiling point of FC-72 is appropriate for electronic cooling applications, much of the pool boiling research for FC-72 has been focused on enhanced surfaces at atmospheric conditions. Rainey et al. [6, 7] utilized micro porous surfaces and micro porous surfaces with fins to enhance the heat transfer rates from pool boiling of FC-72. An additional consideration for boiling of FC-72 is the high temperature overshoot that often accompanies boiling inception due to the low surface tension of the fluid. For example, You et al. [8] reported FC-72 pool boiling incipience wall superheats approaching 50 K on electronic materials. For these reasons, a lot of attention in literature has been given to eliminate the temperature overshoot frequently observed with highly wetting fluids [9-13].

The objective of the present study is to compare the thermal transport characteristics of FC-72 and deionized water for a fixed saturation temperature under identical geometric and flow conditions. The performance of these two working fluids are compared under two cooling schemes corresponding to a base case of pool boiling and a forced convective enhancement by way of submerged impinging jet. Comparison of performance with the latter cooling scheme illustrates whether or not there is a benefit of using forced convective schemes for one fluid relative to the other. Table 1 provides the salient properties of these fluids at the particular experimental conditions considered, where it is noted that water is tested at sub-atmospheric pressure of 0.176 bar in order to achieve a saturation temperature of 57 ^oC. Using a one-dimensional thermal resistance model, the experimental

results are used to compare direct immersion/impingement cooling of FC-72 with water heat sink cooling of a multi-chip module geometry.

While numerous studies exist on pool boiling heat transfer with either water or FC-72, few studies have compared both fluids at identical conditions of interest to the electronics cooling. Saylor et al. [14] introduced several fluid Figures-of-Merit (FOMs) to compare the heat transfer capabilities of water and several dielectric fluids including FC-72. FOMs were derived from governing equations of different cooling schemes for single-phase and boiling heat transfer modes. The author's found that the FOMs for water were at least an order of magnitude superior than the rest of the fluids considered and concluded that water is the best coolant when only considering the thermal aspects. Unfortunately, stringent chemical and electrical requirements often imposed on the liquid coolants for direct immersion cooling drive the attention to fully-fluorinated fluorocarbons such as FC-72. Due to the low latent heat of vaporization of these fluorinated fluids, Saylor et al. [14] recommended to operate in the subcooled state for boiling heat transfer. When considering boiling flows, the authors also recommended taking careful consideration of the incipience wall superheat required to initiate boiling and the maximum attainable heat flux, also known as the Critical Heat Flux (CHF).

A comparison of the thermal performance of a dielectric fluid and water at a fixed operating temperature has been reported in literature in the context of a two-phase thermosyphon used to cool a Pentium 4 processor. Pal et al. [15] reported a reduction in average thermal resistance by 2.4 times for water in comparison to that of a dielectric fluid PF5050, a fluid with almost identical properties as those of FC-72. The improved thermal performance of water was mainly attributed to the fluid thermo-physical properties.

Jet impingement boiling is considered in this paper as a means to enhance direct liquid immersion phase-change cooling (i.e., pool boiling) in electronics thermal management. Several studies on jet impingement boiling in the context of metals processing have been reported in literature, e.g. [16, 17]. For the metals processing application, a water jet typically issues into air prior to impinging on the surface, a configuration referred to as free-surface jet impingement. Studies on jet impingement boiling pertaining to electronics cooling have typically considered a

submerged or confined jet configuration. The submerged jet configuration consists of a liquid jet issuing into a pool of the same liquid prior to impingement, and is used as an enhancement over direct immersion schemes of chip cooling [18-21]. Confined jet impingement consists of a jet issuing into a channel, one wall of which is to be cooled. This configuration has been studied in the context of advanced convective heat sink designs [22, 23]. A submerged jet impingement configuration is presented in this paper as a means of enhancing the immersion cooling (pool boiling) scheme.

Experimental Methods

The experimental facility is described in detail in Cardenas [24] and is shown schematically in Fig. 1. Briefly, the facility consisted of a central chamber within which the pool of fluid, the jet nozzle, and the heated surface were housed. A dedicated vacuum system was used to maintain the sub-atmospheric pressure for deionized water experiments. Condensation coils and pool fluid temperature loops ensured that the pressure and fluid temperature were constant during experiments. Two cartridge heaters were located within the chamber and were immersed in the pool. These heaters were used to degas as well as to maintain pool temperature, which was kept at saturated conditions throughout the experiments. The jet flow was provided by a loop consisting of a gear pump, and the flow rate was monitored using a Coriolis flowmeter. The flow entered the chamber into a plenum prior to exiting to the pool via a 1.16-mm diameter circular nozzle, which was located normal to the test surface. This jet diameter was selected since prior experiments indicated that, for a fixed Re, a 1.16-mm diameter jet resulted in higher CHF magnitudes in comparison to larger jet diameters due to a larger jet exit kinetic energy [21]. The surface-to-nozzle spacing was kept fixed at six jet diameters corresponding to an optimum spacing for peak single-phase jet impingement heat transfer, although Wolf et al. [16] report a weak dependence of nozzle-to-surface spacing on unconfined jet impingement boiling heat transfer. The jet loop fluid lines were equipped with heaters to ensure that the jet entered the pool at the pool temperature, such that thermal entrainment effects were negligible.

The test section, shown schematically in Fig. 2, consisted of an oxygen free copper cylinder whose upper surface was exposed to the fluid. Cartridge heaters that were located on the bottom face of the copper cylinder provided the requisite heat flux. The side face of the copper cylinder was thoroughly insulated such that the steady state heat flux could be determined from temperature measurements of three axially located thermocouples along the copper cylinder using a steady-state 1-D conduction model. The one dimensionality of the temperature profile along the copper cylinder axis was verified experimentally.

Day-to-day shifts in fully developed nucleate boiling curves have been reported in literature [25]. These changes can be partially mitigated by utilizing stringent surface preparation procedures. Surface preparation procedures similar to those used by Katto and Kunihiro [26], Monde and Katto [17], and Han and Griffith [27] were adopted in this study to minimize day-to-day variations in results. Before a day of testing, the heat transfer surface was sanded by hand using powder-free nitrile gloves. The sanding was accomplished through a circular clock-wise movement of the thumb while apply uniform pressure onto the surface. Silicon carbide emery paper of 600, 800, 1200, and 1500-grit were used progressively going down in roughness (up in grit size) to attain uniform sanding levels. Between each sanding level, the surface was cleaned with compressed air and the gloves were changed to avoid contamination from the prior sanding dust. After sanding, the surface was cleaned using acetone and a cotton pad followed by rinsing with deionized water. The surface was then blown dry using compressed air. The final surface finish after sanding was characterized by a high resolution optical profiler to be of an average surface roughness of 33 nm with a 12 percent repeatability uncertainty [24].

Prior to experimentation, the test fluid was thoroughly degassed and the dissolved oxygen content was measured using a dissolved oxygen sensor manufactured by Extech Instruments (Model 407510, accuracy error of ±0.4 ppm). The measured oxygen content for water was lower than the accuracy of the meter used. For FC-72, the dissolved oxygen content measured after the degassing procedure was on average 2 mg/L (0.13×10^{-4} moles/mole). For comparison, the study by You et al. [8] for pool boiling of FC-72 reported a nominal dissolved gas content after degassing of 0.2×10^{-3} moles/mole.

Data of pool and jet temperatures, pool pressure, flow rate, and the copper cylinder thermocouples were recorded throughout the duration of the experiment. High-speed backlit imaging was performed through one of the transparent side windows of the test chamber to augment the heat transfer data. The heater power was incremented in small steps (typically 2 percent voltage steps) and sufficient time was provided at each power level for the system to reach steady state operation. The steady state condition was determined by the independence of the recorded data with time. Once steady state was achieved, one additional minute was permitted for the data acquisition program to collect steady state data. Upon nearing critical heat flux, the electrical power increments were reduced as necessary in order to approach CHF slowly and to reduce the severity of CHF caused by sudden transients in electrical power. CHF conditions were determined by a sudden large increment in surface temperature accompanied by wall heat flux degradation. At this point, the power to the copper cartridge heaters was cut immediately. For the sub-atmospheric water tests, the chamber was immediately depressurized as well to ensure that the surface would not be damaged as a result of the higher CHF values for this fluid.

Table 2 provides a list of the experimental conditions considered in this work. The jet Reynolds numbers (Re) were varied for FC-72 from 0 (pool boiling) to 14000 and for water from 0 to 7000. Corresponding jet exit velocities are provided in Table 2. The Re was chosen as the key hydrodynamic parameter to compare heat transfer performance for consistency with all the existing literature in single-phase jet impingement heat transfer. The lower limit of Re/velocity for water was a result of the limitation of the pump. The performance of the fluids was compared at five conditions of nearly identical Re of 0, 2000, 3725, 5525, and 6960.

Data Analysis Methods and Uncertainty Estimates

The surface heat flux, q'', was calculated from three temperature measurements collected axially along the copper test section using a one-dimensional steady state heat conduction model,

$$q'' = -k\frac{\Delta T}{\Delta x} \quad (1)$$

where k is the copper thermal conductivity, ΔT is the temperature difference between two axial thermocouples inserted inside the copper rod, and Δx is the corresponding spacing between the thermocouples (see Fig. 2). The copper thermal conductivity used in the model was evaluated at the average temperature between the two thermocouple measurements. Three different values of heat flux were calculated from the three temperature measurements and their corresponding spacings. These different values of heat flux were within 0.1 percent of each other in the nucleate boiling regime. The thermocouple closest to the heated surface, located 3.81 mm below the surface, was used to determine the surface temperature using the heat flux value from Eq. 1. Reported values of heat flux and wall superheat correspond to filtered data using a Locally Weighted Scatterplot Smoothing (LOWESS) filter [28, 29], which best represent the steady state average measurements. Details on data filtering can be found in [24].

The jet exit Re was computed based on the jet exit velocity and the local liquid fluid properties,

$$\mathrm{Re} = \frac{\rho_l V_j d_j}{\mu_l} \quad (2)$$

where ρ_l is the liquid density of the working fluid, V_j is the jet exit velocity, d_j is the jet nozzle inner diameter, and μ_l is the liquid viscosity of the working fluid. Fluid properties for water at sub-atmospheric pressures were obtained using Engineering Equation Solver (EES, Fchart software) while FC-72 data at atmospheric pressure were obtained from temperature dependent relationships given by 3M [30] and tabulated values given in [3].

Thermocouples were calibrated using a NIST-traceable RTD and the pressure transducer was calibrated using a NIST absolute pressure calibrator (Omega, PCL-MB) as standards. The Coriolis flow meter (Micromotion Elite II, CMF010 and 2700 transmitter) that measured the mass flow rate of the jet was factory calibrated. An uncertainty analysis was performed on the measured and determined global variables and is reported in Table 3. The Kline and McKlintock method [31] was used to propagate errors from measured to calculated variables in EES. Uncertainty in reported temperatures, pressure, and flow rate included thermocouple bias and precision errors, pressure bias

and precision errors, and flow rate bias and precision errors. Uncertainty in reported heat flux included calibration curve fit error in the temperature difference, average precision error of the thermocouples during the experiments, spacing uncertainty, and uncertainty in thermal conductivity. Single-phase heat transfer coefficient uncertainty is taken from the regression analysis standard fit error of the slope of the single-phase section of the boiling curves.

Data reproducibility was studied by performing repetitions and replications of experiments. During repetitions, nominal operating conditions were re-established following an experimental run (repetition experiments were at least 4 hours apart from each other). During replications, the fluid in the test chamber was drained, the nozzle to surface spacing was readjusted, the surface was re-sanded, freshly degassed fluid was introduced, and nominal operating conditions were re-established (replication experiments were more than 12 hours apart). In general, good agreement was seen between boiling curves from repetition and replication experiments (see details in Cardenas [24]). The most sensitive condition, CHF, varied between four and six percent during repetitions and replications indicating acceptable levels of variability with the experimental procedures adopted. However, for FC-72, boiling incipience superheat and thus the magnitude of the temperature overshoot, which occurred as a result of the low surface tension of the working fluid, was not repeatable. Boiling incipience wall superheat temperatures for pool boiling of FC-72 have been reported in literature to vary widely for identical test conditions and predictions of incipience superheat has been deemed very difficult and have been tackled using a probabilistic approach [8, 21].

Qualification of the experiments was performed by comparing saturated pool boiling CHF data of water and FC-72 with Kutateladze's correlation,

$$q''_{CHF,sat,pool} = Ch_{lv}\rho_v\left[\frac{\sigma g(\rho_l-\rho_v)}{\rho_v^2}\right]^{1/4} \quad (3)$$

with C value of 0.149 as recommended for a large horizontal surface [32]. For FC-72, three reproducibility experiments of pool boiling CHF were on average 14.8 W/cm^2 with variations within six percent. This CHF value is within eight percent of the 16 W/cm^2 predicted by Kutateladze's pool boiling CHF correlation in Eq. 3. As a

reference, reported pool boiling CHF values in literature for saturated FC-72 on plain copper surfaces at atmospheric conditions have varied between 12.6 W/cm^2 [33] and 16 W/cm^2 [34]. For water, the pool boiling CHF from three reproducibility experiments was on average 54.6 W/cm^2 with variations within four percent. This CHF value is within 9.6 percent of the 60.4 W/cm^2 predicted by Eq. 3. Note that while the predicted CHF values were within 10 percent of the experimentally determined values, the correlation over predicted CHF for both cases. CHF for pool boiling has been shown to be dependent on surface finish because surface roughness can alter the wetting characteristics of the surface by the liquid, thereby affecting CHF [35]. Jones et al. [36] reported an increase in CHF with larger surface roughness for pool boiling of FC-77 on aluminum surfaces indicating that CHF dependence on surface roughness is important. For the experimental results presented in this manuscript, the surface roughness average was 33 nm, which is a typical value for a polished metal surface [36]. Therefore, the lower experimental CHF values in comparison to the predictions from Eq. 3 are mainly attributed to the highly polished heat transfer surface being considered. Further details on the effect of surface roughness on CHF for the particular test section being considered can be found in [24, 37].

Results and Discussion

Heat transfer performance of FC-72 and water in pool boiling and jet impingement boiling scenarios are discussed in this section. The section begins with a qualitative high-speed visualization comparison of the pool boiling and jet impingement boiling phenomena for both fluids followed by a discussion of the heat transfer trends. Finally, the section concludes with a simple 1-D heat sink analysis comparing the thermal resistance of a water jet impinging on the surface of a heat sink attached to a silicon substrate to that of direct immersion/impingement cooling of FC-72 on the silicon substrate.

Flow Visualization Comparison

Owing to the significantly lower surface tension of FC-72 compared with water, it is expected that the departing vapor bubbles of FC-72 are smaller than those of water at equivalent pressures. When the pressure of water is

lowered to match the corresponding saturation temperature of FC-72 at P=1 bar, the vapor bubbles are even larger in size. Figure 3 shows a comparison of the vapor bubble sizes for the two fluids in the isolated bubble regime of pool boiling. A significantly larger size of vapor bubbles for water is immediately apparent. Commonly used bubble departure diameter correlations such as that by Cole and Rhosenow (as stated in Carey [35]) indicates that the bubble departure diameter, d_d, is directly proportional to surface tension and inversely proportional to pressure (by the pressure dependency of the vapor density),

$$\left(\frac{g[\rho_l - \rho_v]d_d^2}{\sigma} \right)^{1/2} = C \left(\frac{T_c C_{pl} \rho_l}{\rho_v h_{lv}} \right)^{5/4} \tag{4}$$

In Eq. 4, C is 1.5×10^{-4} for water and 4.65×10^{-4} for fluids other than water. . The saturated vapor density of water decreases with decrease in pressure by 5.1 times from a ρ_v = 0.5897 kg/m^3 at P= 1 bar to a ρ_v = 0.1158 kg/m^3 at P=0.176 bar. A decrease in vapor density implies a larger bubble size for a fixed mass of fluid evaporated per bubble in accordance with the anticipated trend from Eq.4. Surface tension also increases with decrease in saturation temperature contributing to the larger bubble size at departure for water. Intuitively, it would be expected that larger bubbles would lead to premature CHF condition as they tend to coalesce together at the surface and impede the liquid supply. However, as will be seen in the next section, CHF trends do not follow this intuition owing to the significantly larger latent heat of vaporization of water compared with FC-72.

In addition to the significantly different bubble sizes, another key difference between water and FC-72 pool boiling lies in the substantial temperature overshoot required to initiate boiling for FC-72. An important concern in heat transfer is that this overshoot temperature cannot be well predicted and varies with repeats of seemingly identical experiments (e.g. [8, 21, 24]). In the present experiments on jet impingement boiling of FC-72, overshoot variations were also observed to be uncorrelated with jet Re. Once the temperature incipience condition was achieved, the boiling front was seen to spread rapidly over the entire surface at a fixed value of heat flux [21, 24], with the rate of spread of the front being correlated with the superheat temperature at inception [21, 24]. In contrast, no temperature overshoot was observed with deionized water and boiling initiated at regions of high wall superheat.

With increase in heat flux during jet impingement boiling, the manner in which boiling progresses over the surface was also different between the two fluids. Figure 4 shows this progression for water. At lower heat fluxes (Fig. 4a), single-phase heat transfer dominated the regions near impingement and a boiling front is formed in the periphery of the heated surface. With an increase in heat flux, the boiling front progressed inwards towards the impingement point (Fig. 4b). After a certain heat flux value, the entire surface was covered with bubbles (Fig. 4c). Beyond this point, the main role of the jet seemed to be to provide fluid supply to the surface [20]. With further increase in heat flux, the vapor bubbles on the surface coalesced prior to departing as large vapor masses. In contrast, for large boiling incipience temperatures using FC-72, past the inception heat flux, the entire surface is covered in bubbles until CHF is attained [21]. While the boiling front was typically not observed with increase in heat flux for FC-72 jet impingement due to the large temperature overshoot, the front manifested during decreasing heat flux experiments near inception heat flux levels, or during increasing heat flux for small temperature overshoots [21]. Figure 5 presents snapshots of high-speed videos recorded at decreasing heat flux levels for a particular Re of 9316; similar trends are observed at other Re as well. Initially, the entire surface is covered with columns of vapor resulting from merger of bubbles (Figs. 5a-b). With a decrease in heat flux, individual vapor bubbles become more apparent (Figs. 5c - d). At lower values of heat flux (Fig. 5e), a clear boiling front is observed with a single-phase dominated central region. Further reduction in heat flux results in single-phase regime over the entire surface (Fig. 5f).

Heat Transfer Comparison

Figure 6 shows the saturated pool boiling comparison of water and FC-72 for an almost equivalent fluid saturation temperature of 57 ^{o}C (56.6 ^{o}C for FC-72 and 57.3 ^{o}C for water). Note that at any fixed wall superheat, the heat transfer rates from the surface are larger for water than for FC-72. This trend is evident over the entire boiling curve but it is much more significant in the fully developed nucleate boiling region, which is where a phase-change system will typically be implemented for electronics cooling. Note that the boiling heat fluxes for both fluids were closest immediately after the incipience boiling of FC-72 in the superheats ranging from 11^{o}C to 14 ^{o}C. However, with further increase in superheat, the heat transfer rates were significantly larger for water than for FC-72

allowing the former to attain significantly higher CHF magnitude. Note that the increase in CHF for water comes at similar CHF superheat temperatures for both fluids (~ 26.5 ^{o}C). The enhancement in heat transfer rates for water is seen in spite of the significantly larger bubble sizes at sub-atmospheric pressures compared with that of FC-72 (see Fig. 3). Despite the penalty paid in lower heat transfer rates with decreasing pressure [20], the boiling heat transfer characteristics for water remain far superior to FC-72 for an equivalent saturation temperature. Note also that there was no surface temperature overshoot for water while there was more than a 20 ^{o}C temperature overshoot for this particular experiment run of FC-72. Thus, if it is critical that a certain minimum heat flux be removed at a given temperature, as is the case for electronics cooling, it becomes necessary to ensure that boiling has been initiated in FC-72 at the given superheat. Several artificial means to initiate nucleation have been reported in literature for highly wetting fluids such as zero-angle cavities [9], bubble generation from nearby heaters [10, 11], mixing fluids with different saturation temperatures [12], and coating surfaces with carbon nanotubes [13]. These techniques entail additional considerations in the design of the thermal management system for highly wetting fluids such has FC-72.

The inset figure in Fig.6 shows an example of the boiling curve hysteresis observed for pool boiling of FC-72. Note that the significant temperature overshoot observed for increasing heat flux conditions does not exist during decreasing heat flux conditions as a result of the already active vapor cavities on the surface. Similar boiling curve hysteresis was observed during jet impingement boiling with temperature overshoots varying from 19 ^{o}C up to 32 ^{o}C. Other than the boiling curve hysteresis seen as a result of the temperature overshoot at boiling inception, boiling curves for increasing and decreasing heat flux conditions were nearly identical. For brevity, only increasing heat flux boiling curves are presented in this manuscript.

Figure 7 (a-d) show jet impingement boiling curves for saturated water and FC-72 for an almost identical fluid saturation temperature of approximately 57 ^{o}C. Enhancements in the single-phase region of the boiling curves with Re for water (approximately $T_{surf} - T_{sat} < 10^{o}$C) were more significant than for FC-72 owing the superior thermal conductivity of the former fluid. Comparison of the images in Fig. 4 for water jet impingement at Re= 5478 with the corresponding boiling curve in Fig. 7c indicates that heat fluxes conditions of 22 W/cm^2 (Fig. 4a) and 35 W/cm^2

(Fig. 4b) , corresponded to the knee of the boiling curve in Fig. 7c. At the larger heat flux value of 71 W/cm^2, the entire surface was covered with bubbles (Fig. 4c) indicating a fully developed nucleate boiling regime. The slope of the boiling curve is seen to be varying in the partially developed boiling regime while it is relatively constant in the fully developed region. In contrast, no clear distinction in the shape of the boiling curve near inception was observed for FC-72, indicating that during increasing heat flux conditions, fully developed nucleate boiling region existed over most of the temperature superheat range for this fluid under the conditions studied. In the fully developed nucleate boiling region, at any fixed Re in Figs.6 and 7, the slope of the boiling curve is greater for water than for FC-72. A steeper boiling curve slope is highly advantageous in electronics cooling because the chip temperature can be maintained fairly constant over large changes in surface heat flux [13].

A notable difference between pool boiling and jet impingement boiling curves is that the difference in heat flux values between water and FC-72 in the 11-14 ^{o}C superheat range is more significant in jet impingement boiling than in pool boiling. For a fixed wall superheat, the wall heat flux difference between water and FC-72 increases with increasing jet Re. This trend indicates that the benefit of increasing the jet Re is greater for water than it is for FC-72. This result can be partially attributed to the difference in bubble sizes between water and FC-72 (Fig. 3). Since vapor bubbles are much larger in size for water in comparison to FC-72, enhancements in fluid supply to the surface by means of an impinging jet would benefit water to a greater extent than FC-72 since the larger bubbles are more effective in preventing fluid rewetting of the surface during pool boiling.

Table 2 lists values of CHF for water and FC-72 with Re at an equivalent fluid saturation temperature and fixed system parameters. Note from Figs.6 and 7 that CHF values for the two working fluids also occurred at similar surface temperatures. Water CHF limits are seen to be between 3.6 and 4.8 times larger than equivalent CHF limits for FC-72. Figure 8 shows the CHF trends non-dimensionally as enhancement ratios with varying Re for these two fluids. The enhancement ratio is the ratio of CHF at a particular jet Re compared with that of pool boiling of that particular fluid. A plot of enhancement ratio with Re therefore describes whether the utility of a jet is favorable for enhancing the CHF of one fluid compared with the other. As seen in Fig. 8, the enhancement ratios for water were greater than for FC-72 at any given Re, and by as much as 30 percent at Re of 6980. This trend indicates once more

that greater benefits are obtained by using a submerged jet impingement boiling cooling scheme with water than with FC-72. Once again, a comparison of bubble size in Fig. 3 between water and FC-72 provides a plausible explanation for the different enhancement ratios at a given Re. As mentioned in the discussion of Fig. 3, larger bubbles formed under sub-atmospheric conditions with water tend to coalesce together at the surface and form a vapor blanket. The presence of a jet enhances fluid supply to the surface under these conditions thereby delaying the onset of CHF. If it is assumed that, at CHF conditions during pool boiling and jet impingement boiling, the entire energy rate transferred from the surface goes into latent heat, the amount of fluid that effectively undergoes phase-change on the heated surface is larger for FC-72 than for water. Based on the pool boiling CHF, the mass rate of fluid evaporated at CHF is 1.03 g/s for FC-72 and 0.14 g/s for water. Based on jet impingement boiling CHF for Re=6980, the mass rate of fluid evaporated is 1.25 g/s for FC-72 and 0.23 g/s for water. For each fluid, the difference between the mass rate evaporated under jet impingement and pool boiling scenarios provides a measure of the additional mass rate supplied to the surface at CHF by the jet flow. The ratio of this mass rate difference compared to the jet inlet mass rate for FC-72 is 40 percent, while it is only 2.7 percent for water. However, since the latent heat is approximately 27 times larger for water than for FC-72 at the experimental conditions, the dependence of CHF on the amount of fluid supplied to the surface by the jet is more sensitive for water than for FC-72. The rate of change of the enhancement ratio with Re (slope) in Fig.8, which indicates the sensitivity of CHF enhancement with Re, is also greater for water than for FC-72. As seen from Fig. 8, the slope of the curve increases for water with increasing jet Re, while it is almost independent of Re for FC-72 (i.e., there is an approximately linear trend of enhancement ratio with Re).

The boiling curves in Figs. 6 and 7 were used to compute single- and two-phase heat transfer coefficients for the two fluids. For the single-phase region, the slope of the linear portion of the curves was obtained in order to find the heat transfer coefficient. Figure 9 shows the single-phase heat transfer coefficient comparison during jet impingement with FC-72 and water. The solid symbols represent values determined using the well-known Martin's correlation [32]. The experimental data agree with Martin's correlation to within 13.5 percent and 8.5 percent for water and FC-72 respectively. At a fixed Re, significant enhancement in $h_{1\phi}$ is observed for water compared with FC-72, with the $h_{1\phi}$ being 7.3 times larger on average over Re range studied. Figure 10 presents two-phase heat

transfer coefficients, $h_{2\phi}$, obtained by applying Newton's law of cooling to each data point in the boiling region in Figs. 6 and 7, for superheat temperatures of 15 ^{o}C (Fig. 10a) and 20-25 ^{o}C (Fig. 10b). Note that the first superheat corresponds to partially developed nucleate boiling region at all Re for water (see Figs. 6 and 7), wherein the single-phase jet covers a portion of the surface and the periphery is dominated by boiling. Since single-phase heat transfer coefficient is a function of Re, it is anticipated that in the partially developed nucleate boiling region, $h_{2\phi}$also increases with Re as seen in Fig. 10a for water. The trend for FC-72 is seen to be independent of Re, which is also expected since partially developed nucleate boiling was not realized over a significant temperature superheat range for this fluid during increasing heat flux conditions (see Figs. 4 and 7). Also note that with the exception of the lowest Re, $h_{2\phi}$ for water is approximately 3 times larger than that for FC-72. It should also be noted from Fig. 7 that this superheat temperature of 15 ^{o}C is in most cases insufficient to cause boiling inception using FC-72, and that a lower $h_{1\phi}$ could exist in such a scenario for the same superheat temperature (Fig. 9) if boiling were not initiated.

Figure 10b shows that the two-phase heat transfer coefficient is nearly independent of Re for FC-72 and for water up to Re<4000. This is in accordance with literature findings where fully developed jet impingement boiling curves are seen to merge onto a common boiling asymptote [16]. The above trend dominates over the range of Re tested with the exception of the two highest water Re cases at which $h_{2\phi}$ is seen to increase similar to the trend in Fig. 10a. At these higher Re conditions for water, fully developed nucleate boiling conditions would not occur until superheats of approximately 25 ^{o}C. Consequently, $h_{2\phi}$ would increase with Re due to the presence of the single-phase region near the impingement region.

Heat Sink Thermal Resistance Comparison

The boiling curves, enhancement ratios, and heat transfer coefficient data presented in the previous section indicate that water at sub-atmospheric conditions is the fluid of choice for demanding heat transfer applications requiring both low surface temperatures and high levels of heat flux dissipation. However, with the current available technology, it is not possible to reliably bring water in direct contact with electronic surfaces and thus, indirect cooling methods are necessary for this fluid. While it is clear that a significantly larger (3-4 times) amount

of heat can be removed by direct water cooling compared with FC-72, it remains to be seen if the interface thermal resistance is a barrier to this enhanced convective thermal transport. As mentioned before, since it is difficult to keep water dielectric, the fluid should be isolated from the electronic component by constraining it within a heat sink. An example to illustrate the difference in total thermal resistance between the fluid and the chip surface is presented in this section. Two configurations of cooling with water are considered and are illustrated schematically in Fig. 11. The first configuration (Fig. 11a) consists of a jet impingement heat sink that is located on top of a cap that encloses the chip, while the second configuration (Fig. 11b) comprises an integrated heat sink with the chip. The walls of the heat sink are considered to be made of 150-micrometer-thick stainless steel 316L which would provide excellent compatibility with the fluid [38]. This material would also illustrate worst case scenario for heat transfer due to the low thermal conductivity of the material. The cap is considered to be either made of a 0.25-mm-thick copper (k=400 W/m-K) or a 0.25-mm-thick silicon nitride ceramic (k=20 W/m-K). The chip is positioned on a substrate and is affixed to the cap by means of a thermal interface material (TIM). The heat sink is affixed to the cap by means of a second TIM. Three different types of TIMs are considered- grease, gel, and 2 sided carbon nanotube (CNT) arrays [39]. Values of thermal resistances for these interface materials are taken to be constant at 10, 8 and 4 mm^2-K/W respectively [39, 40]. Although data is provided for Si-CNT-CNT-Cu interface [40], it is assumed that the same values would hold good for Si-CNT-CNT-SS316L interface. For the configuration provided in Fig. 11a, five thermal resistances exist for heat to be transferred from the chip surface to the cooling fluid. The first four are conduction resistances of TIM1, cap, TIM2, and heat sink wall. The last resistance is that of convective phase-change pool boiling/jet impingement. The integrated heat sink configuration eliminates two conductive resistances by combining the heat sink bottom wall and the cap as shown in Fig. 11b. For the integrated heat sink the integrated cap/wall is assumed to be made of 150-micrometer-thick SS316L.

The total thermal resistances of both heat sink configurations were compared with direct immersion/impingement of FC-72 on the chip. Convective flux resistances, computed as the inverse of the convective heat transfer coefficient, for water and FC-72 were calculated based on averaged thermal resistance values in the 20-25 ^oC superheat temperature range shown as heat transfer coefficients in Fig. 10b. These average thermal resistances corresponded to heat transfer coefficients of 22,420 W/m^2-K and 6,343 W/m^2-K for water and FC-72 respectively.

Figure 12 shows the comparison of the total thermal resistance (in mm^2-K/W) of various configurations. Reductions in total thermal resistance between 1.8 and 2.7 times are obtained by use of the water heat sinks compared to direct impingement of FC-72. A 30 percent decrease in thermal resistance results from use of the integrated configuration (Fig. 11b) compared with the traditional configuration with a Si_3N_4 cap. This difference between configurations reduces to 15 percent with a copper cap. A 17 percent decrease in thermal resistance is seen by changes in TIM from grease to 2-sided CNT in configuration 1. Figure 12 also illustrates the thermal resistance that can be obtained by direct impingement of water, which is on average 45 mm^2-K/W. This resistance represents the lowest value one can expect to have with a water-cooled immersion/impingement system for the conditions studied here using saturated fluid conditions. The total thermal resistance of the best TIM with the integrated configuration (Fig. 11b) is 30 percent larger than this lower limit. The most significant resistance that needs to be reduced in order to get closer to the direct impingement value is the conductive resistance of the integrated cap/HS wall in Fig. 11b due to the low thermal conductivity of stainless steel. If this resistance were reduced by an order of magnitude by development of high thermal conductivity corrosion-resistant materials, the total thermal resistance of the integrated heat sink could be lowered to 50 mm^2-K/W, which is only 10.6 percent larger than that of direct impingement using water. It is to be noted that Ellsworth [38] suggests that brass with low zinc and lead content, as well as copper and bronzes would be suitable with water. These materials provide thermal conductivities between 3 (bronze) and 27 times (for copper) larger than that of SS316L.

While significantly lower thermal resistances have been demonstrated for several heat sinks employing water, the maximum allowable chip surface temperature places a constraint on the allowable heat flux to be dissipated. Figure 13 shows the chip surface temperature, as predicted using the 1-D resistance model, as a function of various heat fluxes for some of the different water heat sinks that were compared in Fig. 12. Also shown for reference is the estimated chip surface temperature for direct impingement cooling of FC-72 at 15 W/cm^2. Chip surface temperatures using an integrated heat sink, a heat sink with a copper cap, and a heat sink with a ceramic cap have been compared against direct impingement cooling using water. It is evident that if a chip surface temperature constraint of 85 ^oC is placed, corresponding to today's most stringent temperature limit for advanced silicon dies [1] and memory devices [2], the maximum heat flux that can be dissipated with direct impingement

boiling of saturated water will be restricted to 60 W/cm^2. Clearly, this heat flux limit would be higher for a higher chip surface temperature constraint and the advantage of using water in comparison to FC-72 would be even greater. However, further increases in dissipated heat flux with this temperature constraint can be achieved by enhancing the convective heat transfer coefficient of the phase-change jet flow by either fluidic modifications or by surface enhancements. Fluidic modifications can take the form of an increased jet velocity, use of an array of jets, or by fluid subcooling, while surface enhancements could be in the form of microstructures or roughness. At saturated conditions, the integrated heat sink is able to dissipate only ~45 W/cm^2 under the temperature constraint of 85 ^{o}C. Reduction in the conductive resistance and an increase in fluid subcooling will be more beneficial in such a heat sink as opposed to enhancing convective heat transfer coefficient of the jet flow.

Conclusions

Comparison of heat transfer characteristics between FC-72 and deionized water was presented under pool boiling and jet impingement boiling scenarios. The thermal performance of both fluids was compared under nearly identical fluid saturation temperatures at pool boiling conditions and at four jet exit Re. A simple 1-D thermal resistance analysis was performed to demonstrate the potential for indirect liquid cooling using deionized water as the coolant in comparison to direct immersion/impingement cooling with FC-72 for electronic cooling applications.

Several heat transfer advantages of using deionized water over FC-72 have been identified and are summarized below:

1. Jet impingement boiling heat transfer coefficients with water are between 3.2 and 3.9 times larger than with FC-72.

2. Enhancements in critical heat flux between 3.6 times (for pool boiling) and 4.8 times (for Re= 6980) are observed for water compared with FC-72.

3. The utility of forced convective enhancement using an impinging jet, as identified by the CHF enhancement ratio, is more pronounced for water than for FC-72.

4. No surface temperature overshoot is seen for water at boiling inception, while mitigation of the significant temperature overshoot requires special consideration in the design of phase-change cooling schemes with FC-72.

5. A reduction in overall thermal resistance between the chip and cooling fluid of approximately 2 times is observed for water heat sinks in comparison with direct immersion/impingement cooling using FC-72. Further reductions in resistance can be achieved by use of higher conductivity heat sink materials.

In addition to the above heat transfer advantages, water is more cost effective, environmentally friendly, and non-hazardous. Use of water requires additional considerations and care in the appropriate design of the heat sink that can operate under sub-atmospheric conditions and the requirement that there be no leaks in the cooling system. While heat fluxes of up to ~45 W/cm^2 can be dissipated using sub-atmospheric jet impingement boiling with saturated water as compared to ~20 W/cm^2 using saturated FC-72, further increase in heat flux dissipation causes the chip temperature to raise in excess of 85 ^{o}C. The limit of dissipated heat flux can be enhanced by advances in chip packaging to permit direct water impingement as well as by surface modifications to permit enhanced convective heat transfer coefficients. Also note that higher heat fluxes are anticipated for systems operating under subcooled conditions.

Acknowledgements

Funding for this project was provided by the National Science Foundation under award number 0748249.

Nomenclature

C_p	specific heat at constant pressure [J/kg-K]
d	diameter [m]
g	gravitational constant (9.81 [m/s^2])
h	heat transfer coefficient [W/m^2-K]
h_{lv}	specific enthalpy of vaporization [J/kg]
k	thermal conductivity [W/m-K]
P	pressure [Pa]
q''	heat flux [W/cm^2]
R"	thermal resistance [m^2-K/W]
Re	Reynolds number [$\mathrm{Re} = \frac{\rho_l V_j d_j}{\mu_l}$]
T	temperature [^{o}C]
t	time [s]
V	velocity [m/s]
Pr	Prandtl number [$\mathrm{Pr} = \frac{\mu C_p}{k}$]

Subscripts

1ϕ	single phase
2ϕ	two-phase
b	bubble
c	critical
cap	cap that encloses the packaged chip
chip	chip
CHF	critical heat flux
conv	convective
HS wall	heat sink wall
i	incipience
j	jet
l	liquid
pool	pool
surf	surface
sat	saturation
TIM	thermal interface material

v	vapor

Symbols

μ	dynamic viscosity [N-s/m^2]
ρ	density [kg/m^3]
σ	surface tension [N/m]

References

1. Bar-Cohen, A., Geisler, K., “Cooling the Electronic Brain,” Mechanical Engineering (ASME Magazine), 133(4), pp.38-41, 2011.

2. Assembly and Packaging White Paper on System Level Integration, “The next Step in Assembly and Packaging: System Level Integration in the Package (SiP).” SiP White Paper V9.0

3. I. Mudawar, "Assessment of High-Heat-Flux Thermal Management Schemes," IEEE Transactions on Components and Packaging Technologies," 24(2), pp. 122-141, 2001.

4. Robinson, “A Thermal-hydraulic Comparison of Liquid Microchannel and Impinging Liquid Jet array Heat Sinks for High Power Electronics Cooling,” IEEE Transactions on Components and Packaging Technologies, 32, (2), pp. 347- 357, 2009

5. Pal, A. and Joshi, Y., "Boiling of water at subatmospheric conditions with enhanced structures: Effect of liquid fill volume," Journal of Electronic Packaging, 130(1), (2008).

6. K.N. Rainey, S.M. You, “Effects of heater size and orientation on pool boiling heat transfer from microporous coated surfaces”, Int. J. Heat Mass Transfer 44 (14) (2001) 2589–2599.

7. K.N. Rainey, S.M. You, S. Lee, “Effect of pressure, subcooling, and dissolved gas on pool boiling heat transfer from microporous, square pin-finned surfaces in Fc-72”, Int. J. Heat Mass Transfer 46 (1) (2003) 23–35.

8. S.M. You, A. Barcohen, T.W. Simon, “Boiling incipience and nucleate boiling heat-transfer of highly wetting dielectric fluids from electronic materials”, IEEE Trans. Comp. Hybrids Manuf. Technol. 13 (4) (1990) 1032–1039.

9. S. J. Reed, I. Mudawar, "Elimination of Boiling Incipience Temperature Drop in Highly Wetting Fluids Using Spherical Contact with a Flat Surface," International Journal of Heat and Mass Transfer, 42(13), pp. 2439-2454, 1999.

10. A. E. Bergles, C. J. Kim, "A Method to Reduce Temperature Overshoots in Immersion Cooling of Microelectronic Devices," Proc. Thermal Phenomena in the Fabrication and Operation of Electronic Components: I-THERM '88, InterSociety Conference on, pp. 100-105, 1988.

11. S. H. Bhavnani, S. E. Balch, and R. C. Jaeger, "Control of Incipience Hysteresis Effects in Liquid Cooled Electronics Heat Sinks," Journal of Electronics Manufacturing, 9(2), pp. 179-190, 1999.

12. P. J. C. Normington, M. Mahalingam, T. Y. T. Lee, "Thermal Management Control without Overshoot Using Combinations of Boiling Liquids," Components, Hybrids, and Manufacturing Technology, IEEE Transactions on, 15(5), pp. 806-814, 1992.

13. Ujereh, S., Fisher, T., Mudawar, I., “Effects of carbon nanotubes arrays on nucleate pool boiling,” Internatinal Journal of Heat and Mass Transfer, 50, pp. 4023-4038.

14. J.R. Saylor, A. Bar-Cohen, T.Y. Lee, T.W. Simon, W. Tong, and P.S. Wu, “Fluid Selection and Property Effects in Single- and Two-Phase Immersion Cooling”, Vol. 11, pp. 557-565, IEEE Transactions on Components, Hybrids, and Manufacturing Technologies, 1988.

15. A. Pal, Y. Joshi, M. H. Bietelmal, C. D. Patel, T. M. Wenger, "Design an Performance of a Compact Thermosyphon," IEEE Transactions on Components, Packaging Technology, Vil 25(4), pp. 601-607, 2002

16. D. H. Wolf, F. P. Incropera, R. Viskanta, "Jet Impingement Boiling," Advances in Heat Transfer 23, pp. 1-132, 1993.

17. M. Monde, Y. Katto, "Burnout in a High Heat-Flux Boiling System with an Impinging Jet," Int. J. Heat Mass Transfer, 21, pp. 295-305, 1978

18. C. F. Ma, A. E. Bergles, "Jet Impingement Nucleate Boiling," International Journal of Heat and Mass Transfer 29(8) (1986) 1095-1101.

19. D. Zhou, C. F. Ma, "Local Jet Impingement Boiling Heat Transfer with R113," Heat and Mass Transfer 40(6-7), pp. 539-549, 2004.

20. R. Cardenas, V. Narayanan, "Submerged Jet Impingement Boiling of Water Under Subatmospheric Conditions", ASME Journal of Heat Transfer, 134 (2), 020909 (8 pages)

21. R. Cardenas, V. Narayanan, "Heat transfer Characteristics of submerged jet impingement boiling of saturated FC-72," International Journal of Heat and Mass Transfer, 55(15-16), pp. 4217-4231

22. W. Nakayama, M. Behnia, H. Mishima, "Impinging Jet Boiling of a Fluorinert Liquid on a Foil Heater Array, Journal of Electronic Packaging 122(2), pp. 132-137, 2000.

23. I. Mudawar, D. C. Wadsworth, "Critical Heat Flux from a Simulated Chip to a Confined Rectangular Impinging Jet of Dielectric Liquid," Int. J. Heat Mass Transfer 34 (6), pp. 1465-1479, 1991.

24. R. Cardenas, "Submerged Jet Impingement Boiling Thermal Management", PhD Dissertation, Oregon State University, Corvallis, OR, 2011.

25. Ma, C. F., and Bergles, A. E., 1986, "Jet Impingement Nucleate Boiling," International Journal of Heat and Mass Transfer, 29(8), pp. 1095-1101.

26. Katto, Y., and Kunihiro, M., "Study of the Mechanism of Burn-out in Boiling System of High Burn-out Heat Flux," Bull. Jap. Soc. Mech. Engrs, 16 pp. 1357-1366, 1973.

27. Han, C.-Y., and Griffith, P., "The Mechanism of Heat Transfer in Nucleate Pool Boiling - Part I," International Journal Heat Mass Transfer, 8, pp. 887-904, 1965.

28. W. Cleveland, S. Devlin, S., "Locally Weighted Regression - an Approach to Regression-Analysis by Local Fitting," Journal of the American Statistical Association 83(403), pp. 596-610, 1988.

29. M. Schlax, D. Chelton, "Frequency-Domain Diagnostics for Linear Smoothers," Journal of the American Statistical Association 87(420), pp. 1070-1081, 1992.

30. 3M, Fluorinert Electronic Liquid FC-72, 3M Specialty Materials, 2000.

31. R. Moffat, "Describing the Uncertainties in Experimental Results," Experimental Thermal and Fluid Science, 1(1), pp. 3-17, 1988.

32. F. P. Incropera, D. DeWitt, T. Bergman, A. Lavine, Fundamentals of Heat and Mass Transfer, sixth edition , John Wiley, Hoboken, NJ, pp. 447-631, 2007.

33. K. N. Rainey, S. M. You, "Effects of Heater Size and Orientation on Pool Boiling Heat Transfer from Microporous Coated Surfaces," International Journal of Heat and Mass Transfer, 44(14), pp. 2589-2599, 2001.

34. K. N. Rainey, S. M. You, S. Lee, "Effect of Pressure, Subcooling, and Dissolved Gas on Pool Boiling Heat Transfer from Microporous, Square Pin-Finned Surfaces in FC-72," International Journal of Heat and Mass Transfer 46(1), pp. 23-35, 2003.

35. Carey, V. P., Liquid-Vapor Phase-Change Phenomena: An Introduction to the Thermophysics of Vaporization and Condensation Processes in Heat Transfer Equipment, Taylor and Francis, New York 2008.

36. Jones, B., Mchale, J., and Garimella, S., "The Influence of Surface Roughness on Nucleate Pool Boiling Heat Transfer," Journal of Heat Transfer-Transactions of the Asme, 131(12), 2009

37. R. Cardenas, V. Narayanan, "Critical Heat Flux in Submerged Jet Impingment Boiling of Water Under SubAtmospheric Conditions", ASME Journal of Heat Transfer, in print.

38. M. J. Ellsworth, "Thermal Design and Implementation of Robust Liquid Cooling Systems for High Performance Computer Systems," InterPACK2011 tutorial, Portland, OR, July 6-8, 2011.

39. B. A. Cola, "Carbon Nanotubes as High Performance Thermal Interface Materials," Electronics Cooling magazine, April 2010 issue, 2010.

40. B. A. Cola, J. Xu, C. Cheng, X. Xu, T. S. Fisher, H. Hu, "Photoacoustic Characterization of Carbon Nanotube Array Thermal Interfaces," 054313, Journal of Applied Physics, Vol. 101, pp. 1-9, 2007.

Table 1: Comparison of saturated fluid properties

	Water (P=0.176 bar)	FC-72 (P=1.01 bar)
T_{sat} [^{o}C]	57.31	56.6
ρ_l [kg/m^3]	984.5	1594
ρ_v [kg/m^3]	0.1158	13.43
μ_l [kg/m-s]	0.0004862	0.0004377
σ [N/m]	0.0667	0.008024
h_{lv} [kJ/kg]	2360	88
C_{pl} [J/kg-K]	4182	1101
k_l [W/m-K]	0.6383	0.05384
Pr	3.19	8.95

Table 2: Summary of Experimental Conditions[1]

Fluid	P [bar] (T_{sat} [^{o}C])	Re	V_j [m/s]	CHF [W/cm^2]
Water	0.176 (57.3)	0*	0	54.6
		1862	0.84	60.9
		3655	1.64	65.3
		5478	2.44	76.6
		6757	3.03	88.5
FC-72	1.01 (56.6)	0*	0	15.2
		2133	0.51	15.2
		3795	0.90	15.7
		5570	1.32	17.5
		7162	1.71	18.3
		9316	2.21	18.8
		12484	2.97	21
		14216	3.38	21.9

[1] d_j=1.16 mm; H/d_j = 6; average surface roughness = 33 nm

* corresponds to pool boiling

Table 3: Representative measurement uncertainty estimate

Variable	Average Uncertainty
Pressure	± 0.004 bar
Pool Temperature	± 0.5 ^{o}C
Jet Temperature	± 0.4 ^{o}C
Surface Temperature	± 0.8 ^{o}C
Excess Temperature	± 0.9 ^{o}C
Surface Roughness	12 %
Δx	± 0.0635 mm
ΔT	± 0.10 ^{o}C
k	± 1 W/m-K
$h_{1\Phi}$	± 14 W/m^2-K (FC-72) ± 183 W/m^2-K (Water) (T_{surf}-T_{sat})=15 ^{o}C
$h_{2\Phi}$	± 6.4 % 15 ^{o}C <(T_{surf}-T_{sat}) <25 ^{o}C ± 4.3 %
Jet Flow Rate	± 0.9 g/min
Re	± 1 %
V_j	± 0.8 %
CHF (water)	± 0.5 W/cm^2
CHF (FC-72)	± 0.2 W/cm^2
Heat Flux	
1 W/cm^2 - 5 W/cm^2	19.6 % - 3.9%
6 W/cm^2 - 10 W/cm^2	3.3% - 2%
11 W/cm^2 - 15 W/cm^2	1.8% - 1.4%
16 W/cm^2 - 20 W/cm^2	1.2% - 1%
21 W/cm^2 - 25 W/cm^2	1% - 0.85%
26 W/cm^2 - 30 W/cm^2	0.83% - 0.74%
31 W/cm^2 - 190 W/cm^2	0.72% - 0.36%

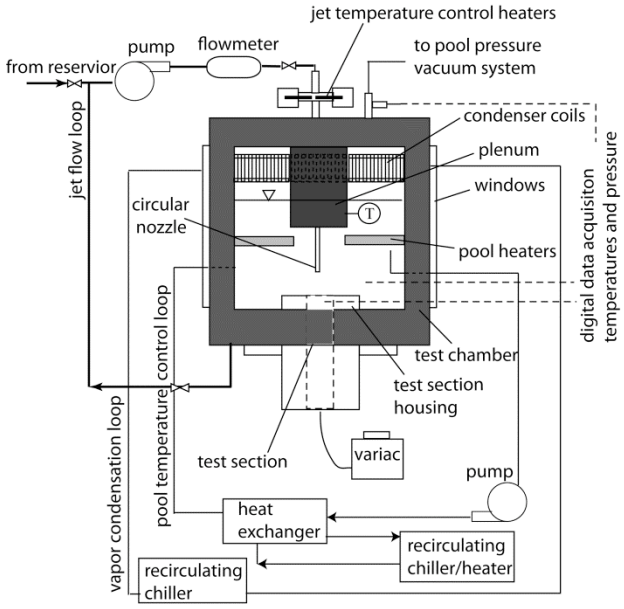

Figure 1: Simplified schematic of the experimental facility.

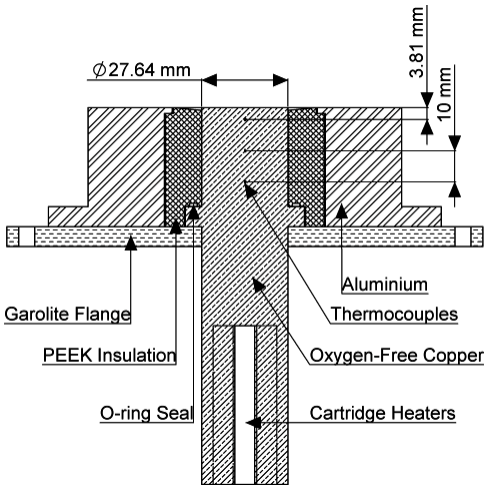

Figure 2: Schematic of test section.

(a) (b)

Figure 3: Comparison of bubble sizes during pool boiling of (a) water at P=0.176 bar and q"= 10 W/cm^2, and (b) FC-72 at P= 1 bar and q'' ~ 1.5 W/cm^2. Note that while the nozzle is seen in the pictures, there is no jet flow.

(a) q"=22 W/cm^2 (29% CHF) (b) q" = 35 W/cm^2 (46% CHF) (c) q"= 71 W/cm^2 (93% CHF)

Figure 4: Visualization of jet impingement boiling of water at various stages of the boiling process at a Re= 5478.

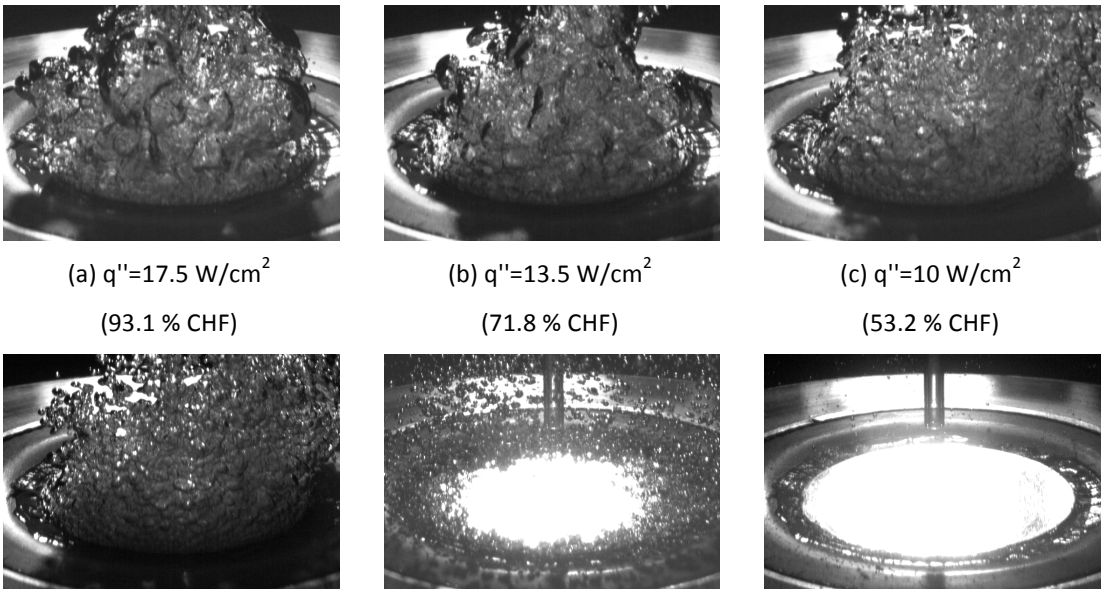

(a) q''=17.5 W/cm^2 (93.1 % CHF)

(b) q''=13.5 W/cm^2 (71.8 % CHF)

(c) q''=10 W/cm^2 (53.2 % CHF)

(d) q''=7 W/cm^2 (37.3 % CHF)

(e) q''=4 W/cm^2 (21.3 % CHF)

(f) q''=2.5 W/cm^2 (13.3 % CHF)

Figure 5: Visualization of jet impingement boiling of FC-72 during decreasing heat flux experiment at a Re=9316.

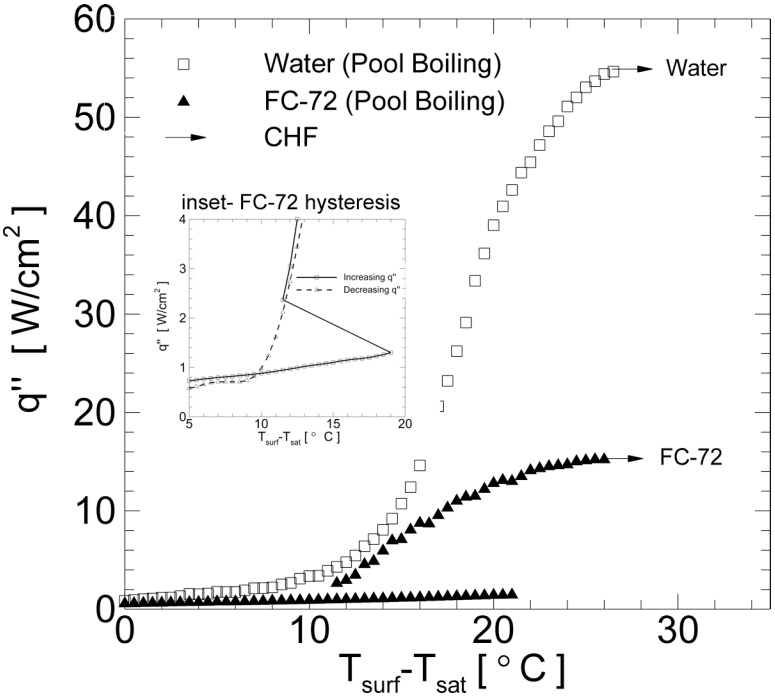

Figure 6: Pool boiling comparison for water at P=0.176 bar and FC-72 on a 33 nm Ra surface.

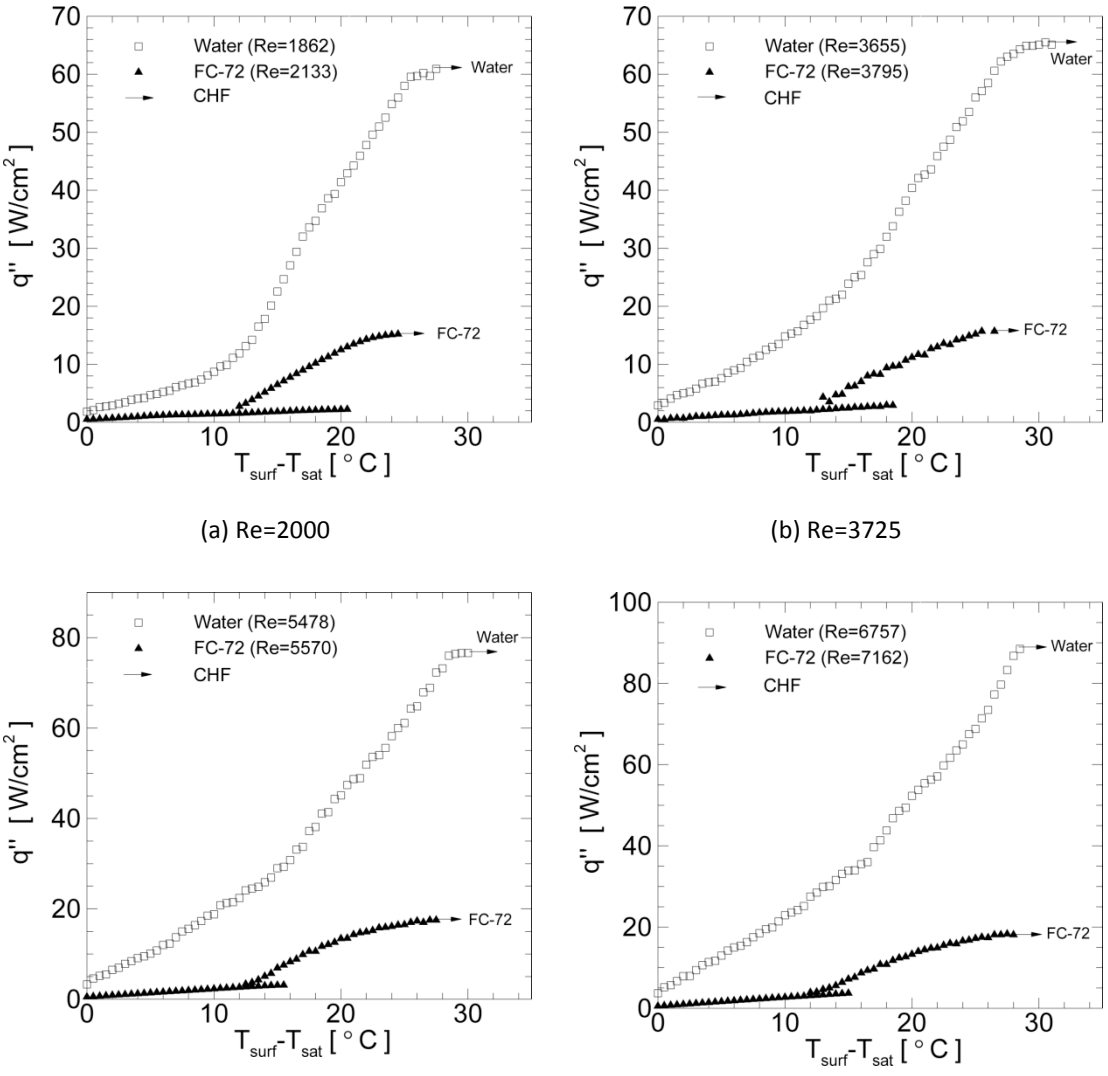

Figure 7: Jet impingement boiling comparison for water at P=0.176 bar and FC-72 on a 33 nm Ra surface.

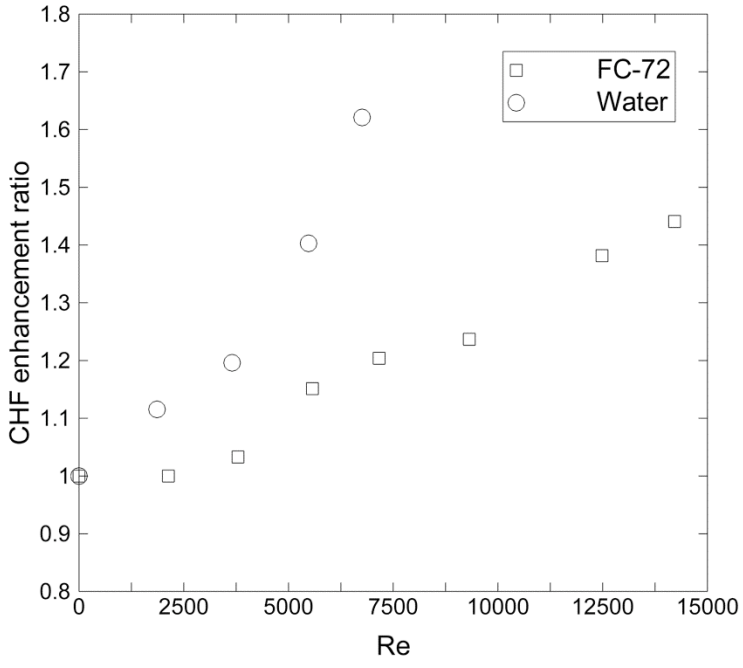

Figure 8: Critical Heat Flux enhancement ratio for water and FC-72 with Re.

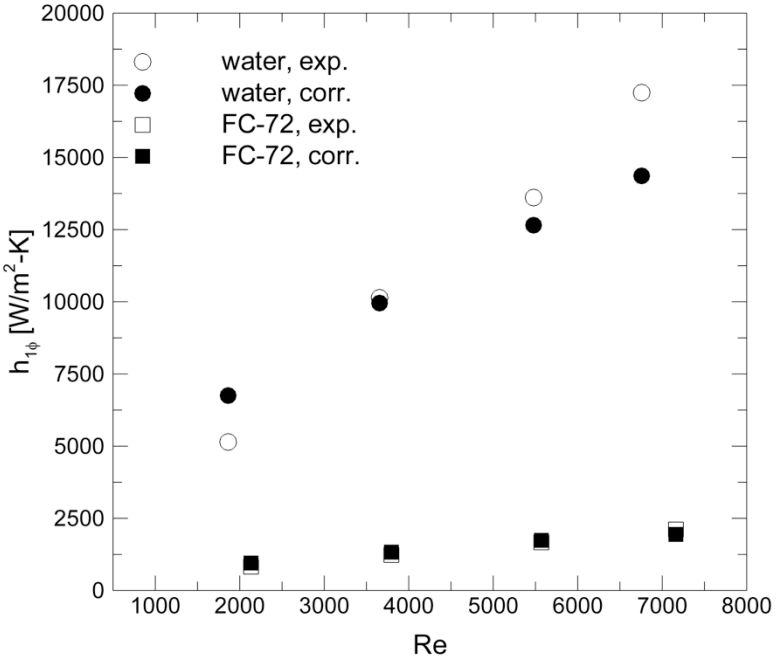

Figure 9: Single-phase heat transfer coefficient comparison of water and FC-72 with variations in Re.

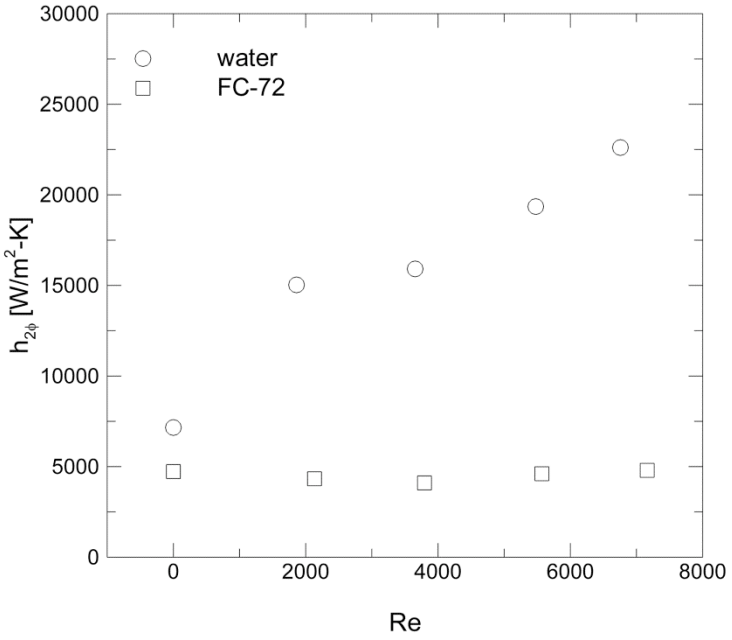

(a)

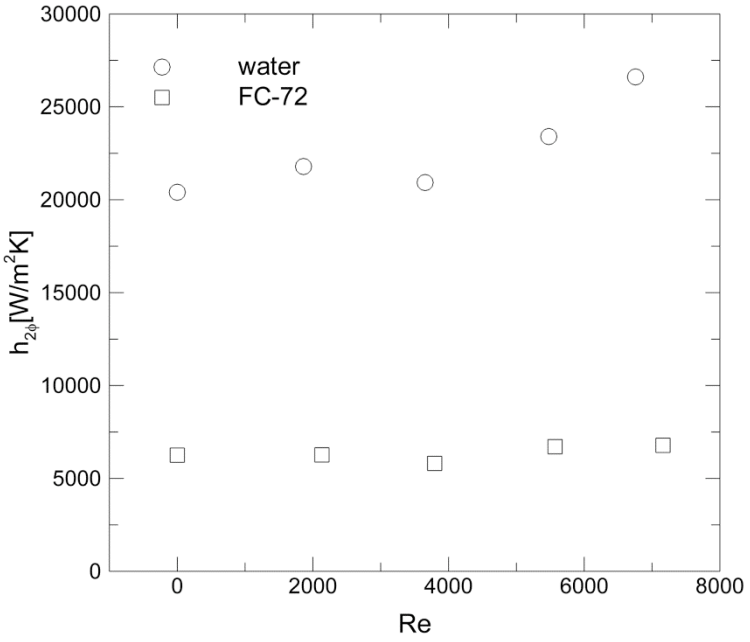

(b)

Figure 10: Nucleate boiling heat transfer coefficient comparison of water and FC-72 with variations in Re for (a) superheat temperature of 15 ^{o}C, and (b) superheat temperatures of 20-25 ^{o}C.

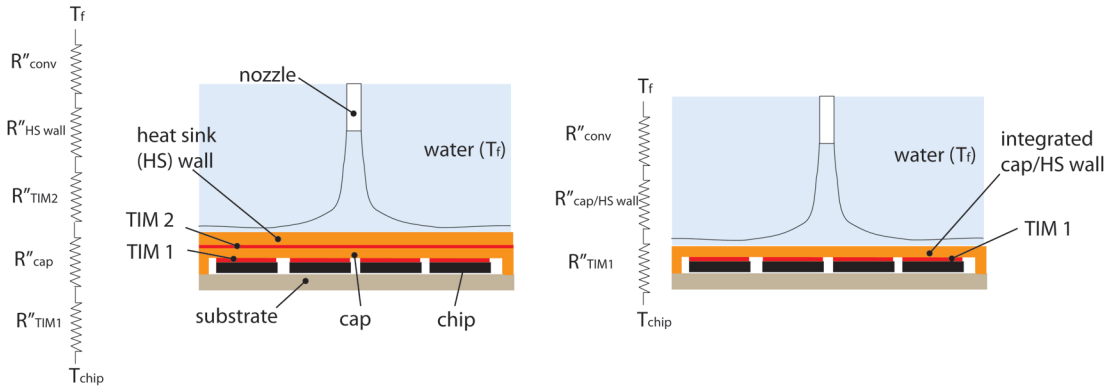

Figure 11: Schematic of 1-D thermal resistance model for deionized water heat sink: (a) cap configuration, and (b) integrated configuration.

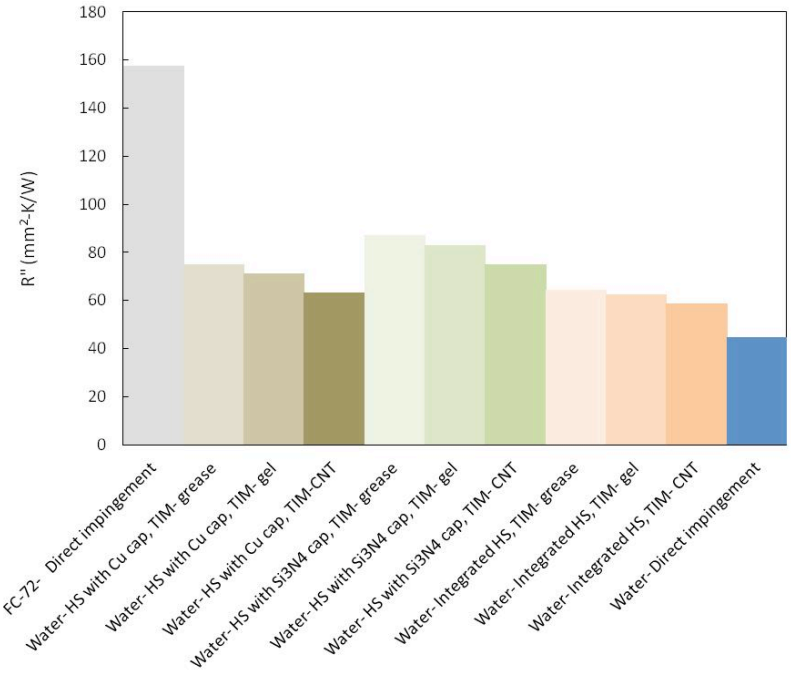

Figure 12: Plot of total thermal resistance, R'', vs. heat sink configuration for water with 3 different TIMs and compared with direct impingement cooling using FC-72 and water.

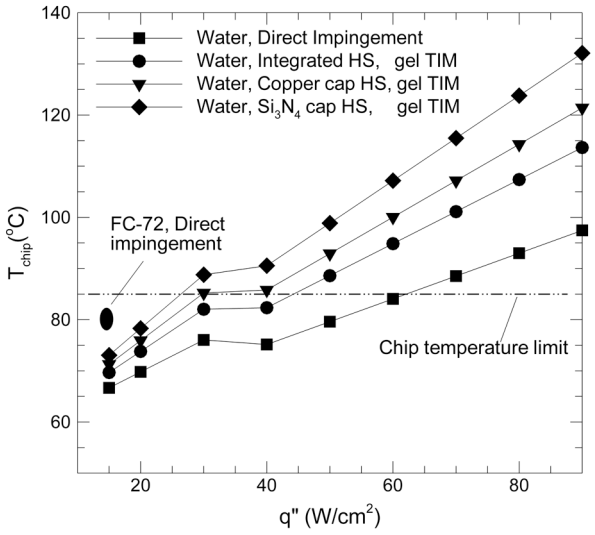

Figure 13: Estimated chip surface temperature as a function of dissipated heat flux for different heat sinks based on a 1-D thermal resistance model.